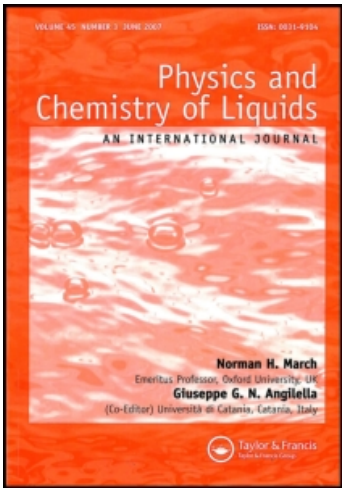

Physics and Chemistry of Liquids
Publication details, including instructions for authors and subscription information:
http://www.informaworld.com/smpp/title~content=t713646857

Effect of Gravity on Contact Angle Hysteresis

M. A. Fortes[a]
[a] Departmento de Metalurgia, Instituto Superior Técnico Av. Rovisco Pais, Lisboa, Codex, Portugal

To cite this Article Fortes, M. A.(1984) 'Effect of Gravity on Contact Angle Hysteresis', Physics and Chemistry of Liquids, 14: 2, 135 — 154
To link to this Article: DOI: 10.1080/00319108408080805
URL: http://dx.doi.org/10.1080/00319108408080805

Phys. Chem. Liq., 1984, Vol. 14, pp. 135–154
0031-9104/84/1402-0135$18.50/0

Printed in the United Kingdom

Effect of Gravity on Contact Angle Hysteresis

M. A. FORTES
Departmento de Metalurgia, Instituto Superior Técnico Av. Rovisco Pais, 1096 Lisboa Codex Portugal

(*Received March 21, 1984*)

The effect of gravity on the stability of equilibrium of a fluid interface in contact with a rough and heterogeneous solid surface is studied for a system with cylindrical symmetry. The equilibrium contact angles measured in relation to the mean solid surface are then evaluated and contact angle hysteresis is discussed. The general effect of gravity is to decrease contact angle hysteresis. The effect depends on the size (width) of the fluid interface. As the size of the fluid interface decreases, it may happen that the advancing contact angle becomes smaller than the receding angle (contact angle inversion). There is also an effect of inclination of the solid surface on hysteresis. The hysteresis behaviour is predicted in detail in limiting cases and by considering a solid surface with sinusoidal grooves.

1 INTRODUCTION

Equilibrium contact angles are central quantities in the characterization of the wettability of solids and in the determination of their surface tensions and surface energies. However, contact angle measurement[1] is made complicated by the fact that different angles are usually determined, depending on whether the equilibrium configuration is reached by advancement of the line of contact solid-liquid-vapour over the dry solid or by retractment of that line from the wetted solid surface. This contact angle hysteresis is attributed[1–4] to the roughness and heterogeneity of actual solid surfaces. It occurs even though the local contact angle is completely determined, through Young's equation, by the local surface tensions of the solid-vapour and solid-liquid interfaces.[5,6]

Several theoretical approaches to the problem of contact angle hysteresis have been undertaken,[3,4,7–9], using simple model systems with either cylindrical or axial symmetry. In only one of these studies[8] has gravity been included, in an analysis of a system with cylindrical symmetry, in which the

liquid surface was of infinite radius of curvature at the apex and contacted a vertical saw-tooth solid surface.

The general outcome of these studies is that the triple line (solid–liquid–vapour contact line) has to make jumps as it is forced to move between equilibrium positions on the solid surface. The jumps occur from different positions in advancing and receding, leading to measured contact angles in advancing that are larger than in receding. This is experimentally observed. The triple line can only occupy a range of stable positions on a rough solid surface, separated by regions where equilibrium is unstable.[4,7,9] For axial and cylindrical symmetry (no gravity) it has been shown[4] that the stable regions are such that the triple line advances on them as the volume of liquid increases. For large symmetric liquid drops (no gravity), the critical points, at the frontiers between stable and unstable regions, coincide with the inflection points of the solid surface propile, stability occuring in the protruding regions between inflection points. This then leads to an hysteresis of the contact angles measured in relation to the mean solid surface. A similar effect occurs if the surface contains regions of different contact angles (heterogeneous surface).

It is experimentally observed (e.g. 10) that both the advancing and receding angles for a drop on a horizontal plate, decrease as the size of the drop decreases. Good and Koo[10] suggested that this effect may be related to the convolutions in the surface of the drop that develop in the vicinity of the solid due to the contorted nature of the triple line on a random rough or heterogeneous surface. Objections to this explanation have been recently raised by the present author.[4]

This paper contains a detailed analysis of the stability of a fluid interface in contact with a rough and heterogeneous surface, under gravity. The inclusion of gravity implies that only the simplest systems can be analysed, because the thermodynamic treatment requires that the shape of the fluid interface is known in closed form. We shall study a system with cylindrical symmetry and with a vertical plane of symmetry, which is analogous to the one analysed by Eick *et al.*[8] We consider, however, a general shape of the solid surface and an arbitrary curvature of the liquid surface. The system is limited by two vertical walls, perpendicular to the symmetry axis, a distance L_0 apart. The contact angle with these walls is assumed to be 90°, so that the cylindrical symmetry is preserved. The following analysis can be regarded as a generalization of the one previously undertaken for a gravity free system.[4]

Predictions on the measured contact angles are made, with special emphasis on the effect of gravity, solid surface inclination and dimensions of the liquid surface. These predictions suggest that contact angles are even more dependent on the particularities of the system in which they are measured than generally admitted.

2 VARIATION OF VOLUME WITH POSITION OF TRIPLE LINE

2a Rough surfaces

The model system to be analysed is schematically shown in Figure 1a–c. To describe the solid surface we take a z-axis vertical upwards with origin at the point where the solid surface intersects the vertical plane of symmetry and a x-axis in the horizontal plane. Because of symmetry we may take $x > 0$.

Two types of solid surfaces will be considered. In type I surfaces, the profile is defined by $z(x)$, implying that there is only one value of z for each x. Type II surfaces are defined by $x(z)$. Examples are shown in Figure 1a–c. Other types of profiles will not be considered. The slope angle at any point, relative to the horizontal, is λ, given by

$$\operatorname{tg} \lambda = \frac{dz}{dx} = \dot{z} = \frac{1}{\dot{x}} \tag{1}$$

where a dot means derivation with respect to the independent variable. Since we require that λ be a continuous function of position, it will be taken in the interval $(-90°, 90°)$ for type I profiles and in the interval $(0, 180°)$ for type II profiles. All calculations will be made simultaneously for the two types; only in the final discussion of stability a distinction has to be made between the two types of profiles.

To describe the fluid interface, $\bar{z}(x)$, we take a $\bar{z}$-axis with origin at the apex and directed downwards. The radius of curvature at the apex is r_0: it is positive if the fluid interface is concave downwards (as in Figures 1a, 1b)

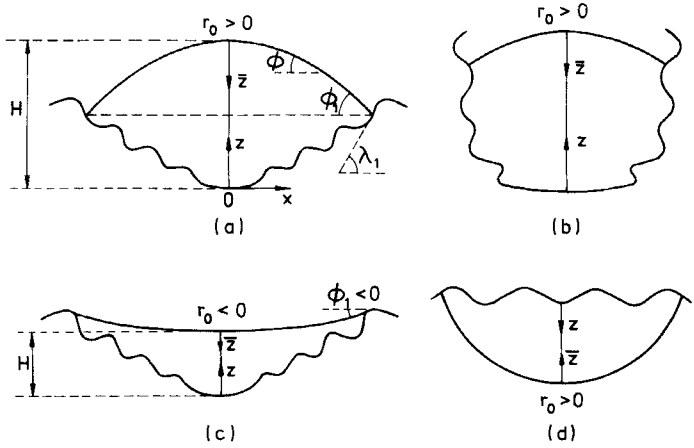

FIGURE 1 Cross-sections of the systems to be analysed: (a)–(c) sessile menisci; (d) pendent meniscus. The solid surface can be of two types: type I is examplified in (a) and (c), and type II in (b). The curvature of the fluid interface is positive in (a) and (b) and negative in (c).

and negative in the other case (Figure 1c). We shall refer specially to the system in Figure 1a, although the equations that we write are applicable in all cases. The slope angle, ϕ, of the fluid interface relative to the horizontal plane is given by

$$\operatorname{tg}\phi = \frac{\mathrm{d}\bar{z}}{\mathrm{d}x}. \tag{2}$$

It is positive in the case of Figure 1a, b and negative in Figure 1c. Only liquid surfaces for which ϕ varies in the interval $(-180°, 180°)$ will be considered.

We now introduce the capillary constant

$$a = \left(\frac{\gamma}{\Delta\rho \cdot g}\right)^{1/2} \tag{3}$$

where γ is the fluid interfacial tension, $\Delta\rho(>0)$ is the density difference between the two fluids, and g is the acceleration due to gravity. We define adimensional quantities in terms of a, which are denoted by a capital letter:

$$X = \frac{x}{a}; Z = \frac{z}{a}; \bar{Z} = \frac{\bar{z}}{a}; R_0 = \frac{r_0}{a}; V = \frac{v}{a^2}. \tag{4}$$

Here $2v$ is the volume of liquid per unit length of the system.

A first integration of Laplace's equation for the fluid interface profile (e.g. 8) leads to

$$-\frac{d}{d\bar{Z}}\cos\phi = \frac{1}{R_0} + \bar{Z} \tag{5}$$

and a second integration to

$$\cos\phi = 1 - \frac{\bar{Z}}{R_0} - \frac{\bar{Z}^2}{2} = f(\bar{Z}). \tag{6}$$

Combining with Eq. 2 we obtain

$$\mathrm{d}X = \frac{f}{(1-f^2)^{1/2}}\mathrm{d}\bar{Z}. \tag{7}$$

All quantities referring to the triple line will be indicated by a subscript 1 e.g., $Z_1, \bar{Z}_1, X_1, \lambda_1, \phi_1$. We have

$$\mathrm{d}Z_1 = \operatorname{tg}\lambda_1 \cdot \mathrm{d}X_1 \tag{8}$$

$$\cos\phi_1 = 1 - \frac{\bar{Z}_1}{R_0} - \frac{\bar{Z}_1^2}{2}. \tag{9}$$

The last equation gives

$$-\sin\phi_1\,\mathrm{d}\phi_1 = -\left(\frac{1}{R_0}+\bar{Z}_1\right)\mathrm{d}\bar{Z}_1 + \bar{Z}_1\frac{\mathrm{d}R_0}{R_0^2}. \tag{10}$$

Differentiating [8] we obtain

$$\mathrm{d}\lambda_1 = k\,\mathrm{d}X_1 \tag{11}$$

where

$$k = \frac{\ddot{Z}_1}{1+\dot{Z}_1^2} = -\frac{\ddot{X}_1}{\dot{X}_1(1+\dot{X}_1^2)} = \frac{a}{\rho_1|\cos\lambda_i|} \tag{12}$$

ρ_1 being the radius of curvature of the solid surface at the triple line.

The reduced volume per unit length is

$$V = \int_0^{Z_1} X\,\mathrm{d}Z + V_M \tag{13}$$

where V_M is the volume of the meniscus per unit length, that is, the volume between the fluid interface profile and a horizontal plane through the triple line. Equilibrium of forces acting on the meniscus, or integration of Eq. 5, leads to

$$V_M + \sin\phi_1 - X_1\left(\frac{1}{R_0}+\bar{Z}_1\right) = 0. \tag{14}$$

Differentiating [13] and [14] we obtain

$$\mathrm{d}V = X_1\,\mathrm{d}Z_1 - \cos\phi_1\,\mathrm{d}\phi_1 + \left(\frac{1}{R_0}+\bar{Z}_1\right)\mathrm{d}X_1 - X_1\frac{\mathrm{d}R_0}{R_0^2} + X_1\,\mathrm{d}\bar{Z}_1. \tag{15}$$

We admit presently that the solid surface is homogeneous. The local contact angle, θ_c, is then independent of position, and related to the interfacial tensions by Young's equation

$$\cos\theta_c = \frac{\gamma_{SV}-\gamma_{SL}}{\gamma}. \tag{16}$$

Since

$$\theta_c = \lambda_1 + \phi_1, \tag{17}$$

we have

$$\mathrm{d}\phi_1 = -\mathrm{d}\lambda_1 \tag{18}$$

Integration of [7] leads to

$$X_1 = \int_0^{\bar{Z}_1} \frac{f}{(1-f^2)^{1/2}}\,\mathrm{d}\bar{Z} \tag{19}$$

which, upon differentiation, gives

$$dX_1 = \text{ctg}\,\phi_1\, d\bar{Z}_1 + I\frac{dR_0}{R_0^2} \tag{20}$$

where

$$I = \int_0^{\bar{Z}_1} \frac{\bar{Z}}{(1-f^2)^{3/2}}\, d\bar{Z}. \tag{21}$$

Finally, we substitute dZ_1 and $d\phi_1$ from Eqs 8, 12 and 18, and eliminate $d\bar{Z}_1$ and dR_0/R_0^2 using Eqs. 10 and 21, to obtain [15] in the form

$$\frac{dV}{dX_1} = k\cos\phi_1 + R_0^{-1} + \bar{Z}_1 + X_1\left[\text{tg}\,\lambda_1 - \frac{R_0^{-1} + k(I\sin\phi_1 + \cos\phi_1)}{I(R_0^{-1} + \bar{Z}_1) + \bar{Z}_1\,\text{ctg}\,\phi_1}\right]. \tag{22}$$

If the meniscus has the concavity upwards, ϕ_1, R_0, Z_1 and I are all negative. This is the general equation giving the variation of the triple line position as the volume changes, under equilibrium conditions (equilibrium shape of the fluid interface and Young's contact angle). For type II solid surfaces we shall require

$$\frac{dV}{dZ_1} = \frac{dV}{dX_1}\,\text{ctg}\,\lambda_1. \tag{23}$$

An equation similar to [22] can be obtained for pendent menisci (Figure 1d)

$$\frac{dV}{dX} = -k\cos\phi_1 + R_0^{-1} - \bar{Z}_1 + X_1\left[\text{tg}\,\lambda_1 + \frac{R_0^{-1} - k(I'\sin\phi_1 - \cos\phi_1)}{I'(R_0^{-1} - \bar{Z}_1) + \bar{Z}_1\,\text{ctg}\,\phi_1}\right] \tag{24}$$

where R_0, $\bar{Z}_1$ and ϕ_1 are positive, and

$$I' = \int_0^{\bar{Z}_1} \frac{\bar{Z}}{(1-g^2)^{3/2}}\, d\bar{Z};\; g(\bar{Z}) = 1 - \frac{\bar{Z}}{R_0} + \frac{\bar{Z}^2}{2}. \tag{25}$$

In this case, the z-axis is directed downwards, so that a given solid surface has the same equation $z(x)$ if it is turned upside-down.

2b Heterogeneous surfaces

If the surface is heterogeneous but cylindrical symmetry is kept, $\theta_c = \theta_c(X)$. The derivation of the previous sub-section can be maintained, except for

Eq. 18, which is replaced by

$$d\phi_1 = -d\lambda_1 + d\theta_c = -\left(k - \frac{d\theta_c}{dX_1}\right) dX_1. \tag{26}$$

That is, Eqs 22 and 24 apply with k replaced by $k - d\theta_c/dX_1$:

$$k \to k - \frac{d\theta_c}{dX_1}. \tag{27}$$

3 STABILITY OF EQUILIBRIUM

In this section we show that stability of equilibrium is simply related to the way the position of the triple line changes as the volume V changes: the stable positions are those for which the triple line advances as the volume increases. This will be shown by calculating the second derivative of the Helmholtz energy A (per unit length), at constant volume, and relating it to dV/dX, calculated at constant contact angle θ_c. The calculations will be done for $R_0 \to \infty$, assuming θ_c to be independent of position. The inclusion of a variable θ_c is not difficult, but consideration of an arbitrary R_0 leads to very complicated equations. Analogous calculations have been undertaken, for any $R_0 < 0$, for the no-gravity case.[4]

We write the following expression for the reduced volume (cf. Eq. 13, 14)

$$V = \int_0^{H-\bar{Z}_1} X\, dZ + X_1\bar{Z}_1 - \sin\phi_1 \qquad (R_0 \to \infty) \tag{28}$$

where

$$H = Z_1 + \bar{Z}_1 \tag{29}$$

is the height of the meniscus relative to the solid (Figure 1).

The Helmholtz energy per unit length of the system, 2A, is the sum of the interfacial energies with the potential energy of the two fluids, for which we take the value zero at $z = 0$. We obtain, using Young's equation (cf. Ref. 7),

$$A = \gamma s - \gamma s_{SL}\cos\theta + \Delta\rho g \int_v z\, dv \tag{30}$$

where $2s$ and $2s_{SL}$ are the lengths of the cross-sections of the fluid and solid–liquid interfaces, respectively, and dv is an area element of the cross-section of the liquid (or volume element per unit length). Note that no term related to the free energy of the walls limiting the length of the system has to be included, since the contact angle with these walls is 90° and therefore no change in A

occurs when the wetted area in them varies. We define

$$A^* = \frac{A}{\gamma a} = \frac{s}{a} - \frac{s_{SL}}{a}\cos\,\theta_c + \int_V \bar{Z}dV \tag{31}$$

and calculate the various terms in this equation. For the first term we write

$$\frac{s}{a} = X_1 + \int_0^{X_1} [(1 + + \dot{\bar{Z}}^2)^{1/2} - 1]\,dX \tag{32}$$

and, since

$$\bar{Z} = 2\sin\frac{\phi}{2}; \dot{\bar{Z}} = \text{tg}\,\phi; dX = \cos\frac{\phi}{2}\text{ctg}\,\phi\,d\phi \tag{33}$$

we obtain

$$\frac{s}{a} = X_1 + 2\left(1 - \cos\frac{\phi_1}{2}\right). \tag{34}$$

For s_{SL} we have

$$\frac{s_{SL}}{a} = \int_0^{Z_1} (1 + \dot{X}^2)^{1/2}\,dZ. \tag{35}$$

The reduced potential energy, $\int_V \bar{Z}\,dV$, is the sum of the potential energy up to the level of the triple line:

$$\int_0^{Z_1} XZ\,dZ \tag{36}$$

with that of the meniscus. The latter can, in turn, be decomposed in the rectangular area of sides X_1 and $\bar{Z}_1$, from the level Z_1, up to H, with a contribution

$$X_1\bar{Z}_1\left(H - \frac{\bar{Z}_1}{2}\right), \tag{37}$$

and (with a minus sign) the area between the level H and the fluid interface, with a contribution

$$-\int_0^{X_1} \bar{Z}\left(H - \frac{\bar{Z}}{2}\right)dX = H\sin\phi_1 + \frac{4}{3}\left(1 - \cos^3\frac{\phi_1}{2}\right) - 2\left(1 - \cos\frac{\phi_1}{2}\right) \tag{38}$$

with the integral evaluated from Eq. 33.

Inserting [34]–[38] in Eq. 31 we obtain

$$A^* = X_1 - \cos\theta_c \int_0^{Z_1} (1 + \dot{X}^2)^{1/2}\,\mathrm{d}Z + \int_0^{Z_1} XZ\,\mathrm{d}Z + X_1\bar{Z}_1\left(Z_1 + \sin\frac{\phi_1}{2}\right)$$
$$- H\sin\phi_1 + \frac{4}{3}\left(1 - \cos^3\frac{\phi_1}{2}\right). \tag{39}$$

We shall now derive an expression for $\mathrm{d}V/\mathrm{d}X_1$. Differentiating [28] yields

$$\mathrm{d}V = X_1\,\mathrm{d}H + \bar{Z}_1\,\mathrm{d}X_1 - \cos\phi_1\,\mathrm{d}\phi_1. \tag{40}$$

From Eqs 8, 29 and 33 we obtain

$$\mathrm{d}H = \mathrm{tg}\,\lambda_1\,\mathrm{d}X_1 + \cos\frac{\phi_1}{2}\mathrm{d}\phi_1 \tag{41}$$

and combining with [40],

$$\mathrm{d}V = X_1\left(\mathrm{tg}\,\lambda_1\,\mathrm{d}X_1 + \cos\frac{\phi_1}{2}\mathrm{d}\phi_1\right) \tag{42}$$

since the other terms are infinitesimal of second order. Under constant contact angle, $\theta_c = \lambda_1 + \phi_1$, and with [11], [18], we obtain from [42]

$$\frac{1}{X_1}\frac{\mathrm{d}V}{\mathrm{d}X_1} = \mathrm{tg}\,\lambda_1 - k\cos\frac{\phi_1}{2}. \tag{43}$$

This equation could of course be obtained directly from Eq. 22, by setting $R_0 \to \infty$, $X_1 \to \infty$ and noting that $I \to \infty$ and $\bar{Z}_1 = 2\sin\phi_1/2$.

We require a different expression for $\mathrm{d}V$. Solving [41] for $\mathrm{d}X_1$ and inserting in [40] we get, noting that $\bar{Z}_1 = 2\sin(\phi_1/2)$ and $\mathrm{d}H$ is infinitesimal of second order,

$$\mathrm{d}V = X_1\,\mathrm{d}H - (\sin\phi_1\,\mathrm{crg}\,\lambda_1 + \cos\phi_1)\,\mathrm{d}\phi_1. \tag{44}$$

We now turn to the Helmholtz energy, A^*. A first differentiation of Eq. 39 gives

$$\mathrm{d}A^* = \left[\mathrm{ctg}\,\lambda_1 - \cos\theta_c\,\mathrm{cosec}\,\lambda_1 + X_1\bar{Z}_1 + 2\sin\frac{\Phi_1}{2}\left(H - \sin\frac{\Phi_1}{2}\right)\mathrm{ctg}\,\lambda_1\right.$$
$$\left. + 2X_1\sin\frac{\phi_1}{2}\right]\mathrm{d}Z_1$$
$$+ \left[\sin\phi_1\cos\frac{\phi_1}{2} + X_1Z_1\cos\frac{\phi_1}{2} + X_1\sin\phi_1 - H\cos\phi_1\right]\mathrm{d}\phi_1$$
$$- \sin\phi_1\,\mathrm{d}H. \tag{45}$$

Introducing (cf. Eq. 41)

$$dZ_1 = dH - \cos\frac{\phi_1}{2}\,d\phi_1 \tag{46}$$

in Eq. 45, and simplifying, neglecting infinitesimal terms in dH, the following result is obtained

$$\begin{aligned} dA^* = \Bigg[& -\operatorname{ctg}\lambda_1 \cos\frac{\phi_1}{2} + \cos\theta_c \operatorname{cosec}\lambda_1 \cos\frac{\phi_1}{2} \\ & + \sin\phi_1 \left(H - \sin\frac{\phi_1}{2}\right)\operatorname{ctg}\lambda_1 + \sin\phi_1 \cos\frac{\phi_1}{2} - H\cos\phi_1 \Bigg] d\phi_1 \\ & + X_1 \left(\bar{Z}_1 + 2\sin\frac{\phi_1}{2}\right) dH. \end{aligned} \tag{47}$$

At constant volume, $X_1\,dH$ can be taken from Eq. 44 and we finally get

$$\begin{aligned} \frac{dA^*}{d\phi_1} = & -\operatorname{ctg}\lambda_1 \cos\frac{\phi_1}{2} + \cos\theta_c \operatorname{cosec}\lambda_1 \cos\frac{\phi_1}{2} + \sin\phi_1 \sin\frac{\phi_1}{2}\operatorname{ctg}\lambda_1 \\ & + \sin\phi_1 \cos\frac{\phi_1}{2}. \end{aligned} \tag{48}$$

At this stage, we may check that equilibrium occurs for $\lambda_1 + \phi_1 = \theta_c$, the contact angle condition. In fact, if this condition is introduced in Eq. 48, we find $dA^*/d\phi_1 = 0$, noting that

$$\cos\phi\cos\frac{\phi}{2} + \sin\phi\sin\frac{\phi}{2} = \cos\frac{\phi}{2}. \tag{49}$$

The second derivative of A^* is, from Eq. 48,

$$\begin{aligned} \frac{d^2A^*}{d\phi_1^2} = & -\frac{1}{2}\cos\theta_c \sin\frac{\phi_1}{2}\operatorname{cosec}\lambda_1 \\ & + \operatorname{ctg}\lambda_1\left(\frac{1}{2}\sin\frac{\phi_1}{2} + \cos\phi_1 \sin\frac{\phi_1}{2} + \frac{1}{2}\sin\phi_1\cos\frac{\phi_1}{2}\right) \\ & + \cos\phi_1\cos\frac{\phi_1}{2} - \frac{1}{2}\cos\phi_1\sin\frac{\phi_1}{2} + \operatorname{cosec}^2\lambda_1\,\frac{d\lambda_1}{d\phi_1} \\ & \times\left(-\cos\theta_c\cos\frac{\phi_1}{2}\cos\lambda_1 + \cos\frac{\phi_1}{2} - \sin\phi_1\sin\frac{\phi_1}{2}\right) \end{aligned} \tag{50}$$

Imposing $dV = 0$ (Eq. 42), and combining with Eq. 11, we obtain an equation for $d\lambda_1/d\phi_1$. Inserting this in [50] and simplifying yields

$$\frac{d^2A^*}{d\phi_1^2} = \operatorname{cosec}^2 \lambda_1 \left[\sin \lambda_1 \left(-\frac{1}{2} \cos \theta_c \sin \frac{\phi_1}{2} + \frac{1}{2} \cos \lambda_1 \sin \frac{\phi_1}{2} + \cos \lambda_1 \cos \phi_1 \sin \frac{\phi_1}{2} + \frac{1}{2} \sin \lambda_1 \sin \phi_1 \cos \frac{\phi_1}{2} \right) - k \cos \frac{\phi_1}{2} \operatorname{ctg} \lambda_1 \left(\cos \frac{\phi_1}{2} - \sin \phi_1 \sin \frac{\phi_1}{2} - \cos \theta_c \cos \lambda_1 \cos \frac{\phi_1}{2} \right) \right]. \tag{51}$$

Note that the contact angle condition has not been introduced yet. If we now set $\theta_c = \lambda_1 + \phi_1$, it is easy to show, using simple trigonometric identities, including Eq. 49, that the two terms in curved brackets in Eq. 51 are equal. Simplification of the second of such terms leads to $(\sin \theta_c \sin \lambda_1 \sin \phi_1/2)$, so that we obtain the final result

$$\frac{d^2A^*}{d\phi_1^2} = \cos \frac{\phi_1}{2} \sin \theta_c \frac{\cos \lambda_1}{\sin^2 \lambda_1} \left(\operatorname{ctg} \lambda_1 - k \cos \frac{\phi_1}{2} \right). \tag{52}$$

For type I solid surfaces, $\cos \lambda_1 > 0$; comparing with Eq. 43, we may write

$$\frac{d^2A^*}{d\phi_1^2} = B \frac{dV}{dX_1} \qquad (B > 0) \tag{53}$$

where B is always positive. If the profile is of type II, we have, from Eqs 23 and 43

$$\frac{1}{X_1} \frac{dV}{dZ_1} = 1 - k \operatorname{ctg} \lambda_1 \cos \frac{\phi_1}{2}. \tag{54}$$

Since now $\sin \lambda_1 > 0$, we may write

$$\frac{d^2A^*}{d\phi_1^2} = B' \frac{dV}{dZ_1} \qquad (B' > 0) \tag{55}$$

where B' is always positive.

We recall that $d^2A^*/d\phi_1^2$ is calculated at constant volume and taken for $\lambda_1 + \phi_1 = \theta_c$, while dV/dX_1 and dV/dZ_1 are calculated for $\lambda_1 + \phi_1 = \theta_c$. Equations 53 and 55 then show that equilibrium is unstable when the position of the triple line is such that the volume decreases as this line advances. Where the line advances as the volume increases, equilibrium is stable. The conditions for stable equilibrium are therefore

$$\frac{dV}{dX_1} > 0 \qquad \text{(type I)}; \frac{dV}{dZ_1} > 0 \qquad \text{(type II)}. \tag{56}$$

Note, however, that we have considered only perturbations away from equilibrium for which the shape of the fluid interface conforms to the equation of Laplace. It is unlikely that other perturbations will increase the Helmholtz energy.

The above criterion for stability is the same that was found in a study[4] of gravity free systems with axial and cylindrical symmetry, for any size of the liquid surface. We shall then use conditions [56] and Eqs [22] and [23] to discuss, in the following section, contact angle hysteresis in the system under consideration, for any value of R_0.

4 MEASURED CONTACT ANGLES ON ROUGH SURFACES

If the cylindrical solid surface is rough, we define a mean surface with slope $\bar{\lambda}$ at each point. The slope relative to the mean surface is λ_l, such that

$$\lambda = \bar{\lambda} + \lambda_l. \tag{57}$$

Eventually, $\pm 90°$ has to be added to obtain λ in the required interval. The average value of λ_l is of course zero.

Contact angles are measured relative to the mean surface, when the common optical methods are used. Therefore, if θ^* is the contact angle measured at any position (or macroscopic contact angle, in the nomenclature of some authors, e.g. Ref. 8), we have

$$\theta^* = \phi_1 + \lambda_1 = \theta_c - \lambda_1 + \bar{\lambda} = \theta_v - \lambda_{l1}. \tag{58}$$

As the line of contact is forced to move on the solid surface, positions will be reached, at the limit of stable regions, where the line has to jump to a neighbouring position. The critical positions are those where V reaches a maximum (in advancing) or a minimum (in receding). If λ_a and λ_r are the corresponding slopes, λ_1, the measured contact angles at those positions are

$$\begin{aligned} \theta_a^* &= \theta_c - \lambda_a + \bar{\lambda} \\ \theta_r^* &= \theta_c - \lambda_r + \bar{\lambda}. \end{aligned} \tag{59}$$

Suppose that the solid surface has a periodic rugosity, and to simplify assume first that within a period there is only one critical position for advancing and another for receding. The path of the triple line and the corresponding variation of V with position, X or Z, will be of the type shown in Figure 2a. The angles given by Eq. 59 are the extreme values that can be measured. But it is expected that they will be close to the angles actually measured, provided the wavelength of the rugosity is small compared to the dimensions of the

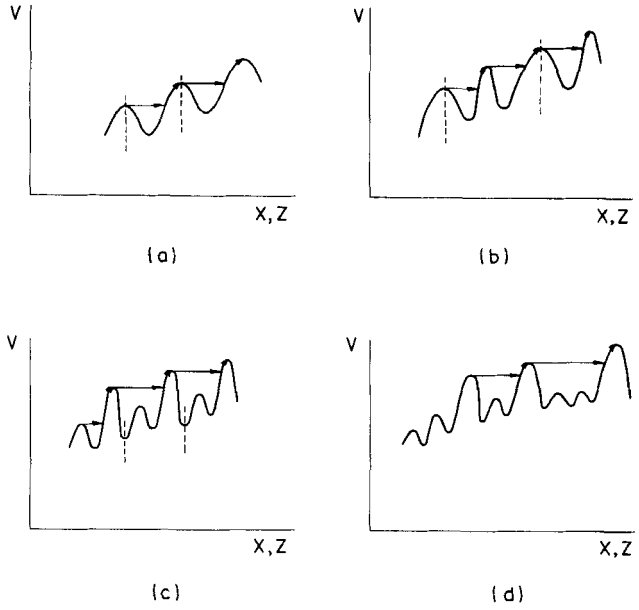

FIGURE 2 Examples of variation of volume, V, with position (X or Z) of the triple line. The arrows indicate the paths for an advancing triple line. (a)-(c) refer to periodic rough surfaces (period marked by dashed lines); (d) refers to a random roughness.

meniscus. In fact, the jumps will then take place to positions which are near to the next maximum or minimum in volume. The advancing path shown in Figure 2a illustrates this.

If n stable regions occur within a period, there will be, within a period, n critical positions both for advancing and for receding. The path of the triple line can be of various types, as shown in Figure 2b, c for $n = 2$. When the volume increases from one maximum to the next as X(or Z) increases, the path is as shown in Figure 2b and the measured advancing angle can be either one corresponding to the maxima. In the other case (Figure 2c), the triple line only "visits" one of the stable regions and the advancing angle has a well defined value. Finally, if the roughness is random (Figure 2d) it is apparent that the measured angles will be controlled by the more prominent maxima and minima.

The critical angles, λ_a and λ_r, can only be evaluated if the surface profile is known. In what follows, a sinusoidal profile[4,7] will be used to illustrate the application of the equations derived above. However, some general predictions can be made in limiting cases, and these will be discussed first.

4a Large liquid surfaces

If the lateral dimension (width) of the liquid surface is very large compared to a, we take $R_0 \to \infty$ and the stability condition [56] becomes (Eqs 43 and 54)

$$\text{tg}\,\lambda_1 - k\cos\left(\frac{\theta_c - \lambda_1}{2}\right) > 0 \qquad \text{(type I)} \tag{60}$$

$$1 - k\,\text{ctg}\,\lambda_1\cos\left(\frac{\theta_c - \lambda_1}{2}\right) > 0 \qquad \text{(type II)} \tag{61}$$

Both condtions are equivalent to

$$\sin\lambda_1 - \frac{a}{\rho_1}\cos\left(\frac{\theta_c - \lambda_1}{2}\right) > 0 \tag{62}$$

which shows that, in general, stability is favoured by large values of $\sin\lambda_1$ and large negative radii of curvature.

We first consider two limiting cases, for large menisci.

1) $a/\rho \to 0$. This corresponds to a very heavy liquid or to an almost smooth surface. In type II surfaces, stability occurs for any position of the triple line; there is no hysteresis, and the line of contact does not jump. In this case, we take for the measured contact angle the average value, which is θ_c. In type I surfaces, the line of contact can only be at regions of positive slope. Jumps will occur from $\lambda_1 = 0$ positions, so that no hysteresis is expected: $\theta_a^* = \theta_r^* = \theta_c$.

2) $a/\rho \to \infty$. Common systems probably fall in this category. Stable positions are in the regions of negative ρ, that is, in protruding regions. The critical positions are those where curvature changes sign, i.e., at the inflection points of the profile, where the slope is maximum or minimum (λ_a and λ_r respectively). From Eqs 59 we conclude that the advancing angle is larger than the receding angle, the difference being $\lambda_r - \lambda_a$ (for type I surfaces, $\lambda_r > 0$ and $\lambda_a < 0$; and for type II surfaces, $\lambda_r > 90°$ and $\lambda_a < 90°$). Since the critical λ_a and λ_r do not depend on the average slope (Eq. 57), it is concluded that no effect of inclination on the measured contact angles is expected in this limiting case.

For intermediate values of a/ρ, the critical positions have to be calculated, from Eqs 60 and 61, for each type of profile. This has been done for a horizontal sinusoidal profile (type I):

$$z = -A\cos\frac{2\pi x}{L} \tag{63}$$

and for a vertical sinusoidal profile (type II):

$$x = x_0 - A \cos \frac{2\pi x}{L} \tag{64}$$

where A is the amplitude and L the wavelength. Note that [63] and [64] define the same solid surface.

Figures 3 and 4 show the stable regions (heavier) in these profiles for various combinations of A/L, a/L and θ_c. All profiles are drawn between two inflection points. The maximum slope λ_l for $A/L = 0.1$ is 32.142° and for $A/L = 1$ it is 80.957°. Table 1 gives the slopes λ_a and λ_r at the critical points and the corresponding values of θ_a^* and θ_r^*. The value of θ_r^* is taken zero when Eq. 59 gives a negative value; and θ_a^* is taken as 180° if Eq. 59 gives a value larger than 180°. Except in one case, there is just one stable region per period.

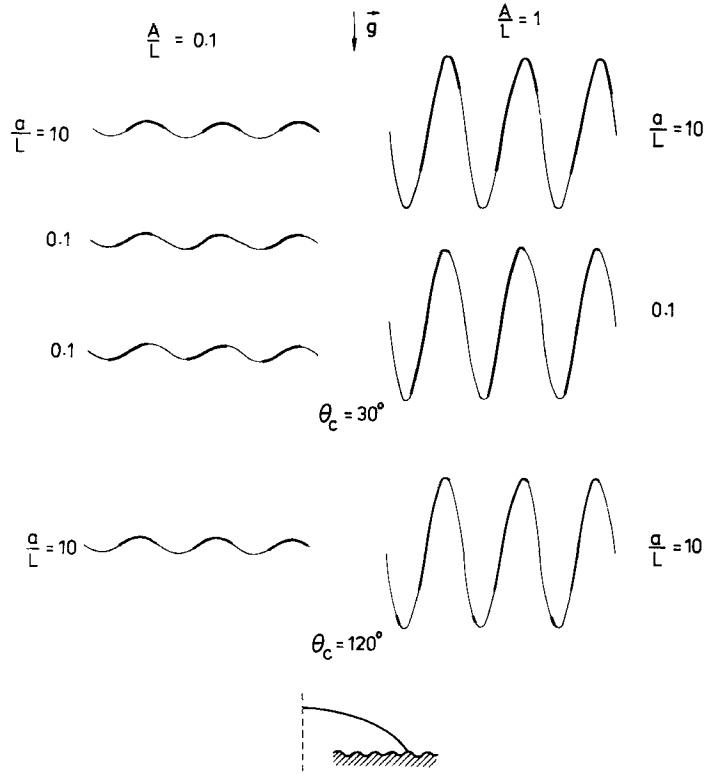

FIGURE 3 Stable regions of the triple line of large menisci in contact with horizontal solid surfaces with sinusoidal profile of wavelength L and amplitude A, for various values of θ_c and of the capillary constant, a. The extreme points of each profile are inflection points. The insert shows the position of the symmetry plane.

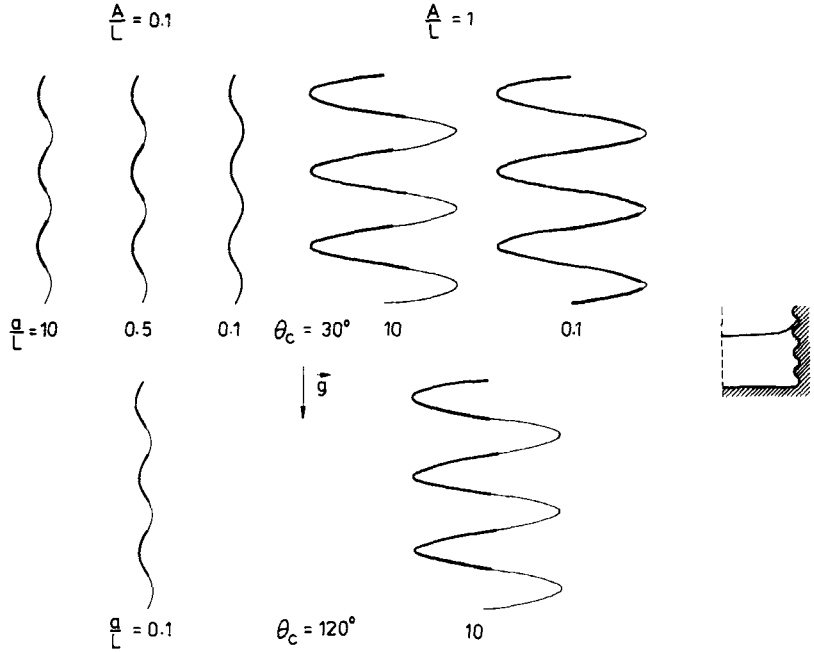

FIGURE 4 The same as in Figure 3, but for a vertical solid surface.

The exception is for the type I profile with $A/L = 1$ and $a/L = 10, \theta_c = 120°$, when a second region is found as shown in Figure 3. However, $\phi_1 > 180°$ in this region, so that it is probably not used by the triple line.

The results obtained confirm the predictions made in the limiting cases previously discussed. Further conclusions are as follows (see Table I).

1) For fixed A/L (same rugosity) the amount of hysteresis, defined as $(\theta_a^* - \theta_r^*)$, increases as a/L increases; θ_a^* increases and θ_r^* decreases.

2) For fixed a/L, hysteresis increases as A/L increases; θ_a^* increases and θ_r^* decreases.

3) For horizontal surfaces $|\lambda_a| < \lambda_r$; for vertical surfaces $\lambda_a < 180° - \lambda_r$ if $\theta_c = 30°$, but $\lambda_a > 180° - \lambda_r$ if $\theta_c = 120°$.

4) Hysteresis is affected by θ_c, with $(\theta_a^* - \theta_r^*)$ apparently decreasing as θ_c increases.

5) There is an effect of inclination on the measured contact angles. For example, for $\theta_c = 30°$, the advancing angle is larger for a horizontal surface than for a vertical surface when $A/L = 0.1$, but the reverse is found for $A/L = 1$. For $\theta_c = 120°$ the differences that occur between horizontal and vertical positions are not simple to describe.

TABLE I

Critical slopes and measured contact angles (degrees) for sinusoidally grooved surfaces.

		Horizontal				Vertical			
$\frac{A}{L}$	$\frac{a}{L}$	$\theta_c = 30°$				$\theta_c = 30°$			
		λ_a	λ_r	θ_a^*	θ_r^*	λ_a	λ_r	θ_a^*	θ_r^*
0.1	10	−32.133	32.135	62.133	0	57.87	122.11	62.13	0
0.1	1	−31.37	31.57	61.37	0	59.60	119.02	60.40	0.98
0.1	0.5	−29.45	30.04	59.45	0	64.97	115.58	55.03	8.42
0.1	0.2	−23.20	24.32	53.20	5.68	—	—	30	30
0.1	0.1	−16.44	17.44	46.44	12.56	—	—	30	30
1	10	−79.00	79.58	109.00	0	9.08	170.65	110.9	0
1	1	−70.05	71.82	100.05	0	11.57	163.92	108.4	0
1	0.1	−50.17	52.57	80.17	0	31.59	140.17	88.41	0
		$\theta_c = 120°$				$\theta_c = 120°$			
0.1	10	−32.10	32.13	152.10	87.87	57.87	122.16	152.13	87.84
0.1	1	−27.23	31.00	147.23	89.00	59.96	120.56	150.04	89.44
0.1	0.1	−9.24	11.56	129.24	108.44	—	—	120	120
1	10	−58.41	79.59	178.41	40.41	9.18	170.90	180	39.10

A—amplitude; L—wavelength; a—capillary constant.

4b Small liquid surfaces

The determination of the stable positions for a meniscus of arbitrary size is too complicated and has not been undertaken. Instead we shall analyse the other limit of size, that of narrow menisci with the dimension x_1 small compared to the capillary constant, a. The stability condition is now, from Eq. 22

$$\frac{1}{a}\frac{\mathrm{d}V}{\mathrm{d}X_1} = \frac{\cos\phi_1}{\rho\cos\lambda_1} + \frac{1}{r_0} > 0. \tag{65}$$

For a horizontal sinusoidal plate (Eq. 63), the region of stability increases as $r_0 > 0$ decreases and, at least for $\theta_c < 90°$, is located in the valleys of the solid surface. Examples of calculated stable regions are shown in Figure 5 for $r_0 = 10a$ ($a = 0.27$ cm for the water–air interface in Earth's gravitational field) and $L = 0.01a$. In some cases, two stable regions develop, but in general the protruding areas are avoided.

When only one stable region occurs, it is found that $\theta_a^* < \theta_r^*$. The inversion of the measured contact angles may even occur for $\theta_c = 120°$, when two stable regions appear, but it is not possible to predict the path of the triple line in this case.

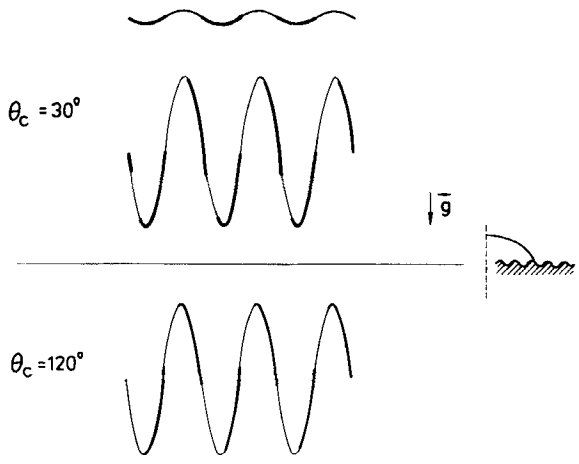

FIGURE 5 Stable regions of the triple line for small menisci with $a/r_0 = 10$, on horizontal sinusoidal surfaces of wavelength L and amplitude A. In all cases $a/L = 100$ ($r_0/L = 10$).

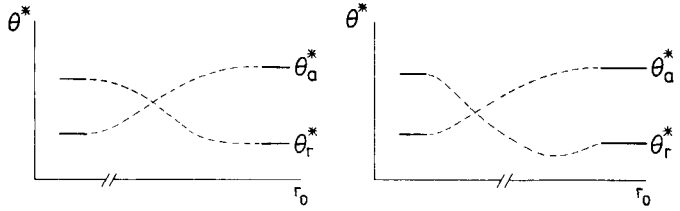

FIGURE 6 Effect of dimensions on measured contact angles (see text).

In the intermediate range of sizes, the variation of θ_a^* and θ_r^* with meniscus dimensions is not simple to predict. Figure 6 shows two possibilities. The curves in Figure 6b confirm to the experimental observation of a decrease in both θ_a^* and θ_r^* as the drop size decreases, but this requires a minimum in the θ_a^* curve. Only a complete calculation of the measured contact angles as a function of size, using Eq. 22, could confirm the occurrence of a minimum in θ_r^*. It certainly does not occur if $a/\rho \to \infty$, because, for large drops, the angles θ_a^* and θ_r^* will have the extreme values of θ^*. Figure 6a is then appropriate to this case.

5 MEASURED CONTACT ANGLES ON HETEROGENEOUS SURFACES

We consider only a planar smooth surface placed horizontally ($z = 0$) and with a heterogeneity described by a fluctuating function $\theta_c(X)$. Equation 22

with k replaced by $-\mathrm{d}\theta_c/\mathrm{d}X$ and $\lambda_1 = 0$ is the basic equation to discuss contact angle hysteresis in this case.

For very large menisci, the stable positions are those for which $\mathrm{d}\theta_c/\mathrm{d}X$ is positive, leading to a normal contact angle hysteresis, not affected by gravity. The advancing angle is near to the maximum θ_c and the receding angle near to the minimum θ_c. As the drop size decreases, θ_a^* must decrease and θ_r^* increase, as in Figure 6a. Stability is now favoured by negative values of $\mathrm{d}\theta_c/\mathrm{d}X \cos\phi_1$. For $\phi_1 > \pi/2$ (acute contact angles) an inversion is expected as the drop size gets very small.

6 CONCLUSIONS

The model system analysed in this paper is certainly far from actual systems, particularly in what concerns the type of rugosity and heterogeneity of the solid surface. However, the conclusions drawn can probably be applied, at least qualitatively, to more realistic systems. Attempts at treating such systems (e.g. 3) meet with enormous difficulties, because even the equilibrium shape of the fluid interface can then only be determined by approximate methods, excluding the possibility of treating the stability problem and therefore contact angle hysteresis.

The relation that we have found between stability and change of the triple line position as the volume changes, is likely to be valid for all systems, although a proof of its general validity seems hard to elaborate.

For large drops and large menisci, the stable positions of the triple line are in the protruding areas of the solid surface, particularly those of large curvature, with gravity favouring the ascendent sides of the protrusions. This explains contact angle hysteresis and indicates that it should be reduced by gravitational fields. This effect of gravity occurs because the stable regions, and therefore the critical positions for the triple line, are altered; it is not an effect on Young's contact angle, which we assumed to be independent of gravity.[6] Heterogeneity alone does not give rise to a gravity effect. It is also interesting to note that contact angles may differ for sessile and pendent drops of the same size and on the same surface, as a comparison of Eqs 22 and 24 indicates.

For small drops or small menisci, there is a tendency to avoid the protruding regions of the solid surface, and this may in some cases originate an inversion in hysteresis, with the advancing angle smaller than the receding angle. Heterogeneity leads to a similar variation of the two contact angles with drop size. However, this variation can hardly explain the experimentally observed decrease of both angles as the size decreases.

The effect of inclination of the solid surface was not studied in detail. Although it may be noticeable in some cases (see Table I), for the common systems used in contact angle measurement (large liqud volumes, large values of a/ρ), the effect is probably a minor one.

Finally, it should be noted that the distinction between roughness and heterogeneity, which is probably artificial,[11] particularly if high curvature regions (e.g. edges) occur in the solid surface, could in principle be avoided by considering, through Eq. 27, an equivalent curvature at each point which incorporates the effect of heterogeneity.

Acknowledgement

This work was supported by Centro de Mecânica e Materiais da Universidade Técnica de Lisboa (CEMUL).

References

1. A. W. Neumann, *Adv. Colloid Interface Sci.* **4**, 105 (1974).
2. R. E. Johnson Jr., R. H. Dettre and D. A. B. Brandreth, *J. Colloid Interface Sci.* **62**, 205 (1977).
3. C. Huh and S. G. Mason, *J. Colloid Interface Sci*, **60**, 11 (1977).
4. M. A. Fortes, in *Physicochemical Aspects of Polymer Surfaces*, K. L. Mittal, Ed., Plenum Press (New York, 1983).
5. L. Boruvka and A. W. Neumann, *J. Phys. Chem.* **66**, 5464 (1977)
6. M. A. Fortes, *Phys. Chem. Liq.* **9**, 285 (1980).
7. R. E. Johnson Jr. and R. H. Dettre, in "Contact Angle, Wettability and Adhesion" *Advanc. Chem. Ser.* No. 43, pg. 112 (1964).
8. J. D. Eick, R. J. Good and A. W. Neumann, *J. Colloid Interface Sci*, **53**, 235 (1975).
9. M. A. Fortes, *Colloids and Surfaces*, **8**, 361 (1984).
10. R. J. Good and M. N. Koo, *J. Colloid Interface Sci.*, **71**, 283 (1979).
11. A. W. Neumann and R. J. Good, *J. Colloid Interface Sci.* **38**, 341 (1972).